



Article

Analysis of Microstructure and Mechanical Properties of Bi-Modal Nanoparticle-Reinforced Cu-Matrix

Fadel S. Hamid ^{1,*}, Omayma A. Elkady ², A. R. S. Essa ^{1,3}, A. El-Nikhaily ¹, Ayman Elsayed ² and Ashraf K. Eessaa ⁴

- ¹ Mechanical Department, Faculty of Technology and Education, Suez University, Suez 43519, Egypt; ahmed.eessa@suezuniv.edu.eg (A.R.S.E.); ahmedeassa1946@gmail.com (A.E.-N.)
- ² Powder Technology Division, Manufacturing Technology Department, Central Metallurgical R & D Institute, 1 Elfelezzat St. Eltebeen, Cairo 11421, Egypt; o.alkady68@gmail.com (O.A.E.); ayman_elsayed_11@yahoo.com (A.E.)
- ³ Mechanical Engineering Department, Egyptian Academy for Engineering & Advanced Technology, Affiliated to Ministry of Military Production, Cairo 3056, Egypt
- ⁴ Nanotechnology Lab El Nozha, Electronic Research Institute (E.R.I.), Cairo 12622, Egypt; ashrafkamal888@hotmail.com
- * Correspondence: fadel.shaban@suezuni.edu.eg

Abstract: Bi-modal particles are used as reinforcements for Cu-matrix. Nano TiC and/or Al₂O₃ were mechanically mixed with Cu particles for 24 h. The Cu-TiC/Al₂O₃ composites were successfully produced using spark plasma sintering (SPS). To investigate the effect of TiC and Al₂O₃ nanoparticles on the microstructure and mechanical properties of Cu-TiC/Al₂O₃ nanocomposites, they were added, whether individually or combined, to the copper (Cu) matrix at 3, 6, and 9 wt.%. The results showed that titanium carbide was homogeneously distributed in the copper matrix, whereas alumina nanoparticles showed some agglomeration at Cu grain boundaries. The crystallite size exhibited a clear reduction as a reaction to the increase of the reinforcement ratio. Furthermore, increasing the TiC and Al₂O₃ nanoparticle content in the Cu-TiC/Al₂O₃ composites reduced the relative density from 95% for Cu-1.5 wt.% TiC and 1.5 wt.% Al₂O₃ to 89% for Cu-4.5 wt.% TiC and 4.5 wt.% Al₂O₃. Cu-9 wt.% TiC achieved a maximum compressive strength of 851.99 N/mm². Hardness values increased with increasing ceramic content.

Keywords: copper; nanocomposites; metal-matrix composites (MMCs); mechanical properties; spark plasma sintering



Citation: Hamid, F.S.; A. Elkady, O.; Essa, A.R.S.; El-Nikhaily, A.; Elsayed, A.; Eessaa, A.K. Analysis of Microstructure and Mechanical Properties of Bi-Modal Nanoparticle-Reinforced Cu-Matrix. *Crystals* **2021**, *11*, 1081. <https://doi.org/10.3390/cryst11091081>

Academic Editors: Walid M. Daoush, Fawad Inam, Mostafa Ghasemi Baboli and Maha M. Khayyat

Received: 25 July 2021

Accepted: 2 September 2021

Published: 6 September 2021

Publisher's Note: MDPI stays neutral with regard to jurisdictional claims in published maps and institutional affiliations.



Copyright: © 2021 by the authors. Licensee MDPI, Basel, Switzerland. This article is an open access article distributed under the terms and conditions of the Creative Commons Attribution (CC BY) license (<https://creativecommons.org/licenses/by/4.0/>).

1. Introduction

Copper strengthening is a current priority due to the pressing need to use it in various applications requiring a balance of properties [1–3]. Metal-matrix composites are most promising in achieving balanced mechanical properties between nano and microstructure materials [4–8]. Copper is used in many industries owing to its low cost, ease of manufacturing, and good corrosion resistance [9]. The main drawbacks of pure copper are its substantial low strength, high coefficient of thermal expansion (CTE), and generally poor mechanical properties [10]. One effective way to overcome these limitations is to reinforce copper with ceramic particles to obtain composites with superior properties. The effectiveness of dispersed particles in matrix strengthening depends primarily on particle characteristics: size, distribution, spacing, thermodynamic stability, and low solubility and diffusivity of its constituent elements in the matrix. Among ceramic particles, alumina nanoparticles have shown outstanding mechanical properties even at high temperatures, as well as low production costs [11,12]. In addition, TiC is an attractive candidate for metallic matrices such as copper (Cu), iron (Fe), aluminum (Al), titanium (Ti), and nickel (Ni) because of its high hardness, high melting point, and abrasion resistance with good

electrical conductivity [12–14]. Due to the aforementioned factors, Cu reinforced with (TiC-Al₂O₃) composites led to a more viable material.

Numerous techniques have been used to fabricate reinforced copper matrix composites (CMCs), including molecular-level mixing (MLM) [15], in situ metallurgy [12,13], flake powder metallurgy [16,17], high-energy ball milling (HEBM) [7,18–20], friction stir processing [21–26], high-pressure torsion [26], and rolling [27–30]. Although these techniques enhanced the mechanical properties of processed composites, they resulted in an inhomogeneous distribution of particle reinforcements within the matrix. Additionally, they have the potential to cause morphological and structural damage, as demonstrated through carbon nanotubes (CNTs) within a copper matrix [31].

The spark plasma sintering (SPS) method, developed recently, is a new technique for synthesizing metal matrix composites. The SPS technique has piqued researchers' interest due to its advantages of sintering at relatively low temperatures, higher heating speeds, shorter processing times, and the absence of pre-compression as in conventional sintering. Thus, the SPS technique enables the fabrication of nanostructured composites without the high grain growth rate associated with traditional sintering methods. As a result, SPS composites exhibit exceptional mechanical properties at room temperature, even at elevated temperatures [32].

To the authors' knowledge, few papers discuss the solid-state spark plasma sintered Cu-Al₂O₃ [33] and Cu-TiC [34–36], respectively. However, no information on the synthesis and mechanical investigation of hybrid Cu-Al₂O₃-TiC through mechanical alloying and SPS techniques have been released. Thus, this work fabricated three separate nanocomposites of Cu-TiC, Cu-Al₂O₃, and hybrid Cu-TiC-Al₂O₃, using mechanical alloying and SPS processing. The influence of the TiC and Al₂O₃ nanoparticles content on the microstructure and mechanical properties of the prepared nanocomposites was also investigated.

2. Materials and Methods

2.1. Materials

Copper (Cu) powder with 99.9% purity (supplied by AlphaChemical, MA, USA) with an average particle size of 10 μm was used as a metal matrix. Alumina (Al₂O₃) nanopowder with 99.7% purity (supplied by Alpha Chemicals, MA, USA) with an average particle size of 50 nm and titanium carbide (TiC) nanopowder with 99.7% purity (supplied by Inframat Advanced Materials, L.L.C., CT, USA) with an average size of 100 nm were used. Both TiC and Al₂O₃ were used as individual/hybrid reinforcement. The Cu powder was mixed with 3, 6, and 9 wt.% of individual/hybrid reinforcement of TiC and Al₂O₃ using a ball milling technique for 24 h. The powders were mixed in a stainless-steel vial and protected from oxidation using highly pure argon gas using a 25:1 ball to powder ratio (BPR), 110 rpm, and a ball diameter of 5 mm. Stearic acid (1.5 wt.%) was used as a process controlling agent (PCA). Figure 1 and Table 1 show the composition of fabricated samples.

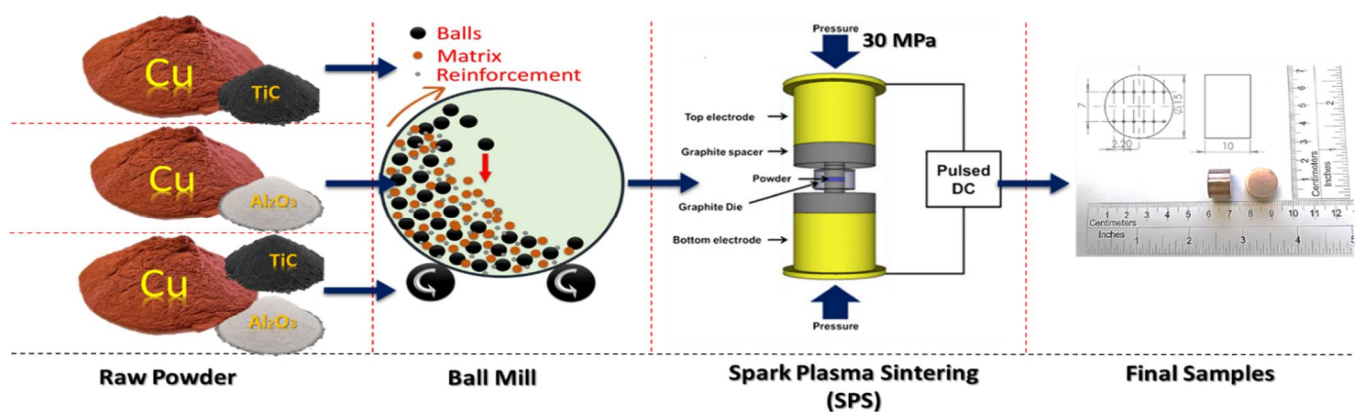


Figure 1. Schematic diagram of Cu with TiC and Al₂O₃ and (TiC + Al₂O₃) hybrid nano reinforcement composites.

Table 1. Composition of the prepared specimens and their contents in the Cu matrix.

	Materials after Sintering by (SPS)	Composition		
		Matrix	Reinforcement	
		Cu [wt.%]	TiC [wt.%]	Al ₂ O ₃ [wt.%]
0	Pure copper	100	—	—
I	Cu-3 wt.% TiC	97	3	—
	Cu-6 wt.% TiC	94	6	—
	Cu-9 wt.% TiC	91	9	—
II	Cu-3 wt.% Al ₂ O ₃	97	—	3
	Cu-6 wt.% Al ₂ O ₃	94	—	6
	Cu-9 wt.% Al ₂ O ₃	91	—	9
III	Cu-1.5 wt.% TiC and 1.5 wt.% Al ₂ O ₃	97	1.5	1.5
	Cu-3 wt.% TiC and 3 wt.% Al ₂ O ₃	94	3	3
	Cu-4.5 wt.% TiC and 4.5 wt.% Al ₂ O ₃	91	4.5	4.5

2.2. Spark Plasma Sintering (SPS)

The sintering process was performed using a spark plasma sintering technique (DR. SINTER LAB Model: SPS-1030, Syntex, Osaka, Japan). In all experiments, the powder was loaded into a graphite die with an inner diameter of 15 mm with graphite foil and enclitic by 0.5 mm thick graphite cover to prevent the friction of the sample with the die during the compaction process and to minimize heat loss. Before sintering, the SPS chamber was evacuated to a pressure below 5 Pa. The samples were heated from room temperature up to 950 °C by pulsed D.C. current using the heating rate of 20 °C/min. The samples were then held at the maximum temperature for 45 min under a uniaxial pressure of 30 MPa applied since the first minute of heating. This processing route was used to fabricate the Cu-TiC/Al₂O₃ nanocomposites.

2.3. Mechanical Properties

The hardness was measured along the polished surface of the specimen using a Vickers hardness tester (HMV-2T Model SHIMADZU, Kyoto, Japan). The test was carried out under 100 g load for 15 s dwell time.

The microhardness values were evaluated for an average of twelve readings on the surface of each sample. The compression test for the investigated specimens was carried out using a universal testing machine. In the compression test, three samples were investigated, and average results were obtained. The dimensions of the specimens for compression tests were 6 mm in diameter and 15 mm in length. The applied crosshead speed was 0.05 mm/s, and the test was performed at room temperature.

3. Results

3.1. XRD Analysis

Figure 2 shows the XRD patterns of the prepared ten samples, pure Cu and 3, 6, 9 wt.% TiC/Al₂O₃ (individual and hybrid) nanocomposites. Only peaks corresponding to Cu, TiC, and Al₂O₃ appeared, whereas pattern-like Cu was observed in the case of 3 wt.% Cu/TiC/Al₂O₃ samples; this may be due to the lower percentage of both TiC and Al₂O₃ that are below the limits of the XRD device. This may be attributed to the controlled milling and sintering process in an argon atmosphere which shows that no other peaks for any new phases or intermetallic compounds were formed due to the rapid consolidation process (45 min) during the SPS technique.

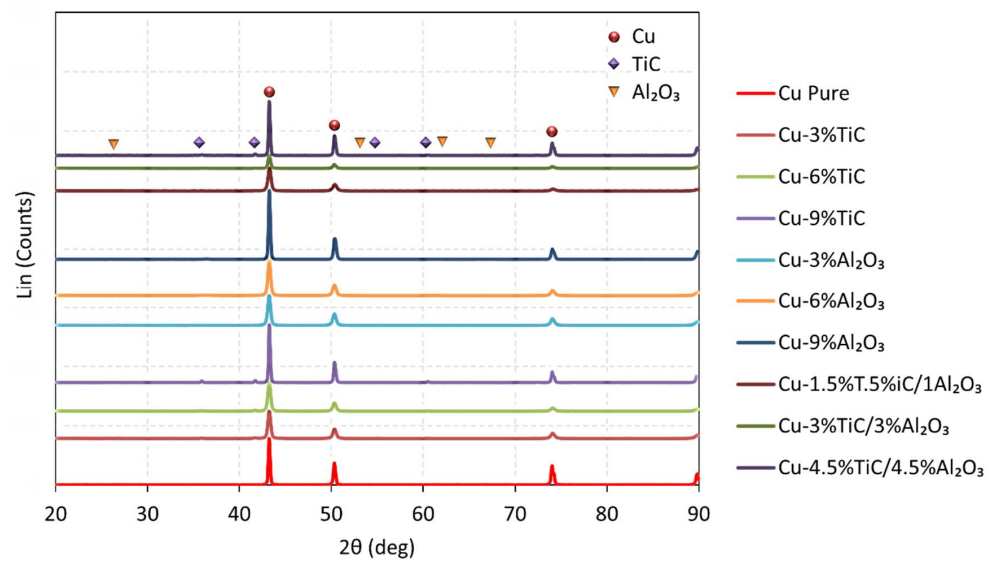


Figure 2. XRD patterns of composites after (SPS) process.

The crystallite size was assessed by the classical Williamson–Hall method (FWHM) from the broadening of XRD peaks and using the following formula [37,38]:

$$\frac{\beta \cos \theta}{\lambda} = \frac{k}{d} + 2\epsilon \left(\frac{2\sin \theta}{\lambda} \right) \quad (1)$$

where β is the full width at half maximum height (FWHM), θ is the Bragg's angle of the peak, λ is the wavelength of X-ray (0.15406 nm), K is a dimensionless shape factor (0.9), which depends on the material, d is the crystallite size, and ϵ is the microstrain.

Figure 3 shows the effect of ceramic ratio on the crystallite size. A clear reduction of the crystallite size with increasing wt.% of ceramic additives was observed. Al_2O_3 and TiC are ceramic materials that act as internal balls that reduce the particle size [39,40]. In addition, the SPS technique achieved the consolidation process, which is a rapid method for the sintering in which no chance for the grain growth of the particles occurs [41,42]. The crystallite size of pure copper was ~ 105 nm, whereas the crystallite size for the produced composites was in the range of 5–25 nm.

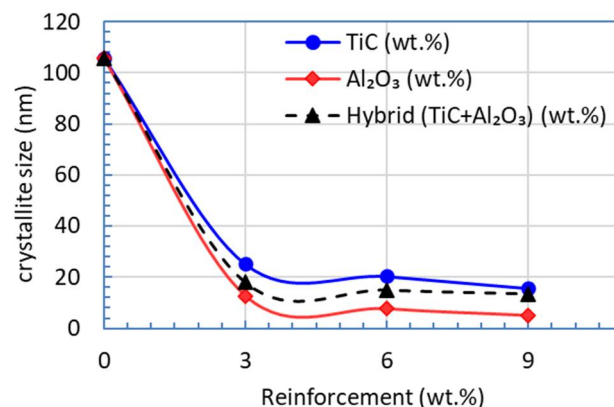


Figure 3. The effect of ceramic additions on the crystallite size.

3.2. Densification

The density of composite material is the most important parameter, which significantly affects both physical and mechanical properties. The relative density is calculated and plotted in Figure 4. Relative density is the ratio of the measured and theoretical density of the sample. Measured density was determined by the Archimedes method, and the

theoretical density was calculated from the simple rule of mixtures. Each percent of pure Cu and 3, 6, 9 wt.% TiC/Al₂O₃ (individual and hybrid) nanocomposite were tested by three samples, and the average results were obtained. It was observed that the relative density decreased with increasing reinforcement content for all composites, as shown in Figure 4. The maximum relative density (~96%) was achieved by adding 3 wt.% TiC to copper, whereas the minimum relative density (89%) was obtained for 9 wt.% Al₂O₃/copper composite. TiC (4.91 g/cm³) and Al₂O₃ (3.987 g/cm³) also have lower densities than Cu [7,35]. So, the addition of a light material to a denser one decreased the overall density of the prepared composites. This may be attributed to the presence of hard ceramic material with a high melting point into a ductile metal such as Cu that may hinder the high densification and increase the porosity content accompanied by the high fraction of reinforcement [7,43].

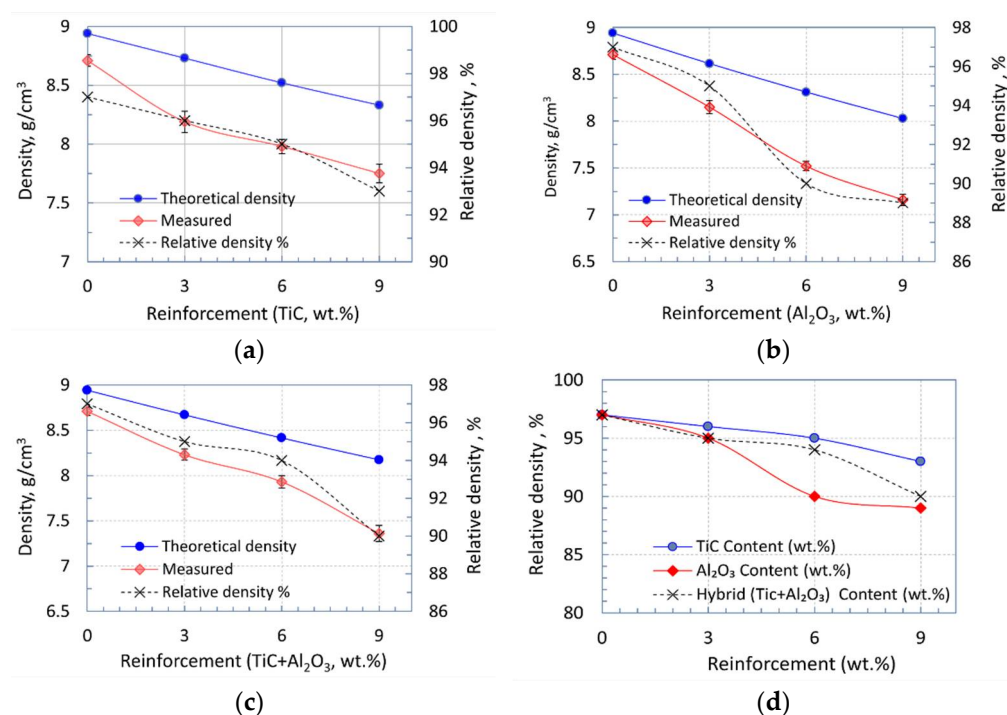


Figure 4. The effect of reinforcement fraction on the density of the produced composites. (a) Cu/TiC composites, (b) Cu/Al₂O₃ composites, (c) Cu/hybrid composite, and (d) Comparison of relative density between three series.

Ayman Elsayed et al. [11] studied experimental investigations for the synthesis of W-Cu nanocomposite through spark plasma sintering, and they concluded that using the SPS technique led to reaching a maximum of 90% relative density. On the other hand, a relative density of 98.1% was reached for Cu-Fe-Al₂O₃-MoS₂ composite sintered using the SPS route [33]. Moreover, Babapoor et al. [44] investigated the effects of spark plasma sintering temperature on the densification of TiC. They reached a relative density of 99.4% at 1900 °C for 7 min under 40 MPa using the TiC powder with a mean particle size of 7 μm. They also suggested that there is an optimum temperature for reaching the maximum density.

3.3. Microstructure Analysis

Figure 5 shows the FE-SEM micrograph of TiC-reinforced copper composite using 3%, 6%, and 9% TiC addition to Cu. Two phases are observed; the dark-gray phase represents the Cu matrix, and the black phase is the TiC particles. For 3 wt.% samples, TiC and Al₂O₃ particles are concentrated along the grain boundaries in a chain form, while 6 and 9 wt.% samples were homogeneously distributed all over the Cu matrix. This may be attributed

to the suitable mechanical milling parameters and good SPS technique applied. The SPS technique leads to a finer structure compared with traditional routes [18,44].

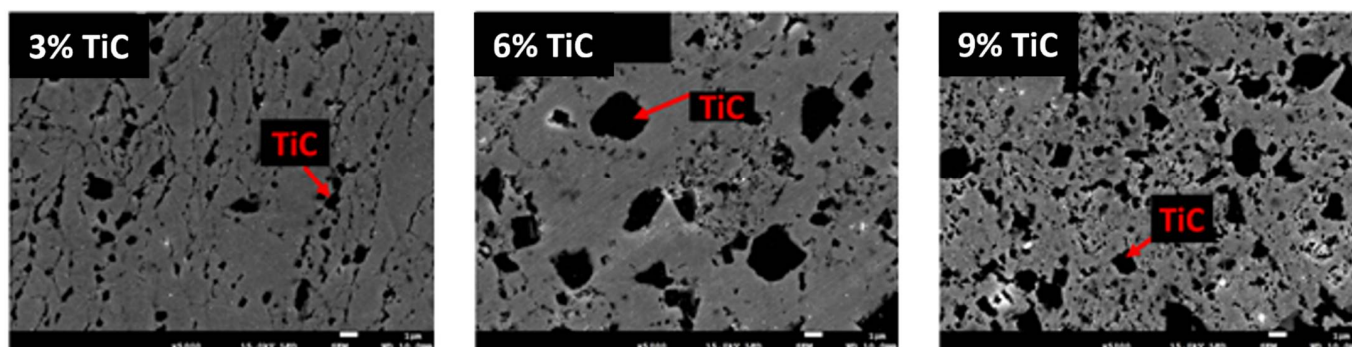


Figure 5. SEM of Cu/TiC nanocomposite with TiC percentage of 3, 6, and 9% prepared using spark plasma sintered route.

The SEM investigation of Cu/ Al_2O_3 microstructure is shown in Figure 6. Two phases are observed; the dark-gray phase represents the Cu matrix while the white phase represents the Al_2O_3 particles. The dispersion of Al_2O_3 inside the copper matrix is observed for Cu/3% Al_2O_3 with a little agglomeration of Al_2O_3 reinforcement. On the other hand, white areas of agglomerated alumina reinforcement are revealed within the Cu/6% Al_2O_3 matrix grain boundaries, whereas very fine particles are dispersed within the grain interior. Moreover, the SEM of Cu/9% Al_2O_3 composite shows that most of the Al_2O_3 nanoparticles are agglomerated along grain boundaries, and a small percentage are dispersed with the grains. Some authors have also concluded that increasing agglomeration steadily occurs, along with increasing the weight percentage of reinforcement [9,15].

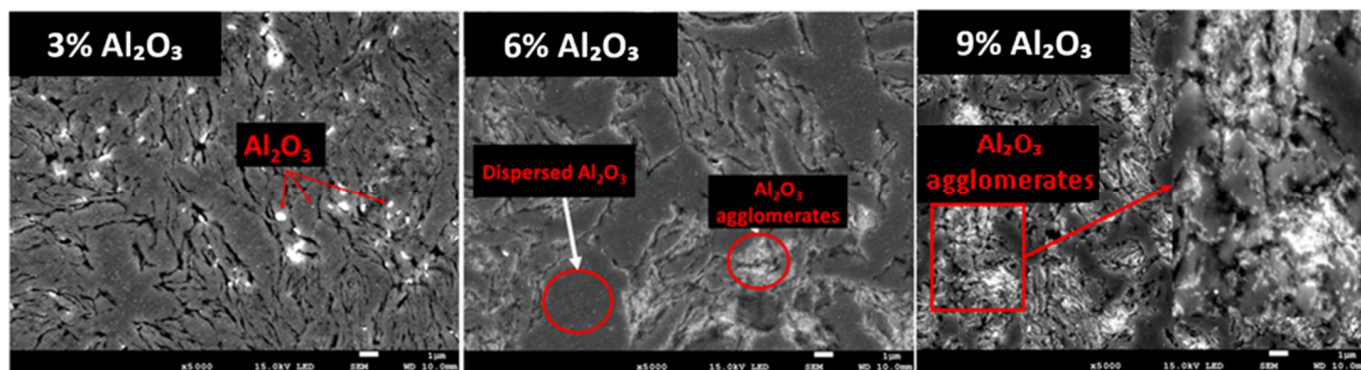


Figure 6. SEM of Cu/ Al_2O_3 nanocomposite with Al_2O_3 percentage of 3, 6, and 9%.

The combination of both TiC and Al_2O_3 for reinforcing copper (Cu/hybrid nanocomposite) with point analysis EDS is shown in Figure 7a,b. The homogeneous distribution of TiC nanoparticles is predominant, while the agglomeration of some Al_2O_3 is observed along grain boundaries. More agglomeration of alumina particles along grain boundaries is observed with increasing hybrid percentage (TiC and Al_2O_3).

3.4. Mechanical Strength

Figure 8 represents the stress–strain curves for pure copper and TiC/ Al_2O_3 -reinforced copper matrix composites, while the key mechanical properties obtained from the compression test are plotted in Figure 9. The compressed samples are photographed in Figure 10. The addition of TiC enhanced the compression strength of copper and reached its maximum compression strength of $\sim 852 \text{ N/mm}^2$ at 9 wt.% TiC, whereas Al_2O_3 additions exhibited a dramatic effect on the Cu strength. Increasing Al_2O_3 from 3 to 6 wt.% increased the Cu strength, but a clear failure of strength is noticed at 9 wt.% ratios at which a minimum value

of compression strength 367.8 N/mm^2 resulted. After the compression test, the Cu-6% Al_2O_3 and 9% Al_2O_3 samples were destroyed (see Figure 10). clearpage

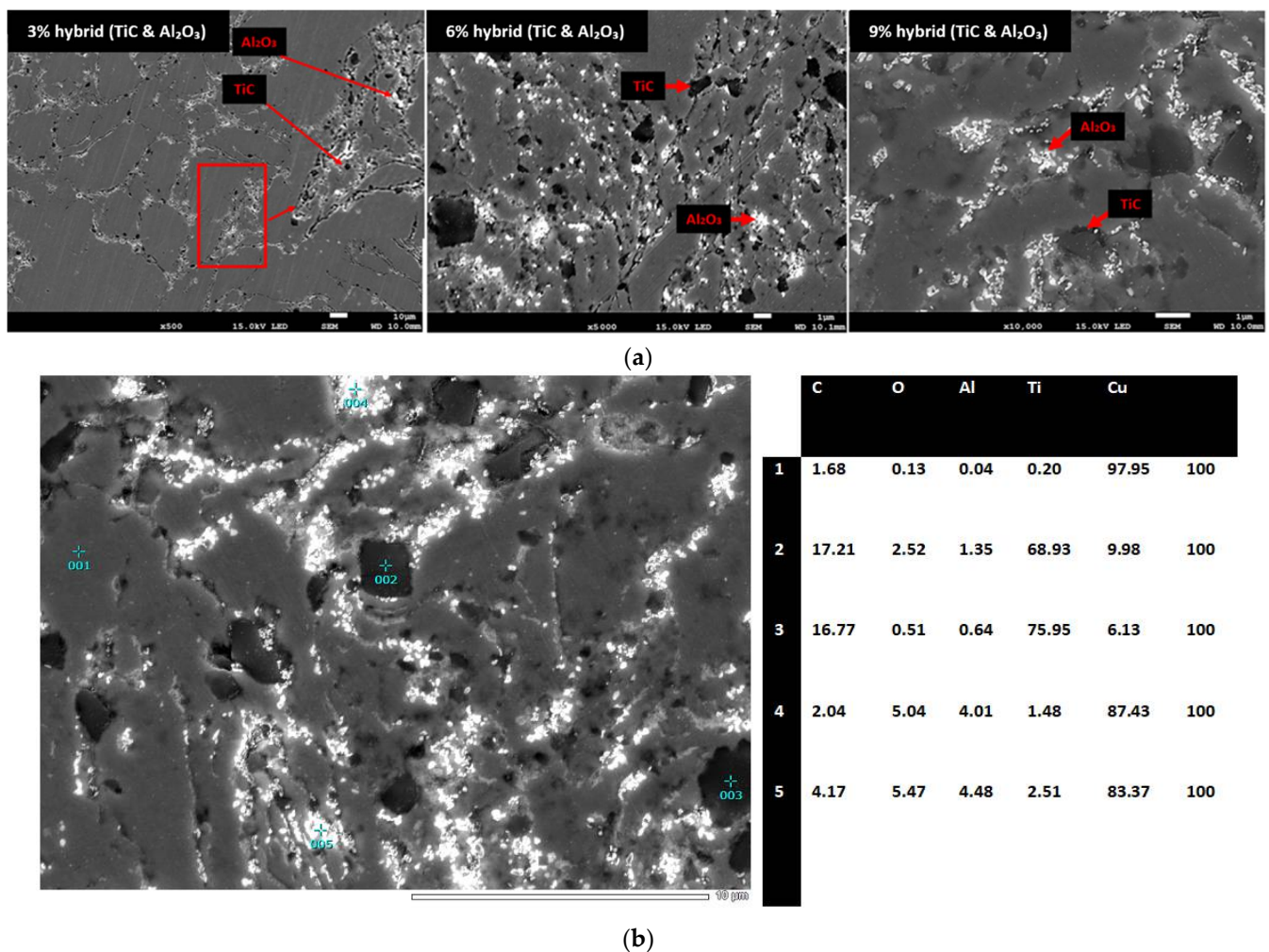


Figure 7. (a) SEM of Cu/hybrid nanocomposite with (TiC+ Al_2O_3) weight percentage of 3, 6, and 9% prepared using the spark plasma sintered route; (b) point analysis for Cu-reinforced hybrid ceramic matrix composite containing 9 wt.% hybrid ratio.

Moreover, the strength of hybrid composites increased firstly with increasing the percentage of reinforcement up to 6% and then slightly decreased. The extreme drop in the compression strength of the Cu/9% Al_2O_3 composite may be attributed to particle-to-particle contact resulting from ceramic particle agglomeration (see Figure 6). The high compression strength of TiC-strengthened Cu prepared by the SPS route compared with Cu/ Al_2O_3 composite with the same wt.% is attributed to a combined effect of ultrafine grain (UFG) structure by the Hall–Petch mechanism and the obstruction of dislocation movement by nanoscale ceramic particles in the grain interior by the Orowan mechanism [8,43].

The effect of ceramic additions on the hardness of copper is illustrated in Figure 11. The hardness steadily increases with increasing the wt.% of reinforcement for synthesized composites. Cu/9% Al_2O_3 obtained the maximum hardness (211 HV), whereas two composites that obtained the minimum hardness value of 112 HV are Cu/3% TiC and Cu/3% hybrid. Many reasons could explain this. The first is that adding high-hardness and high-strength ceramic materials such as TiC and Al_2O_3 on the ductile Cu matrix increases the overall hardness. The second is that the addition of nanomaterials with the incorporation of nanoparticles between the Cu particles improves the hardness as a grain reinforcement takes place accordingly.

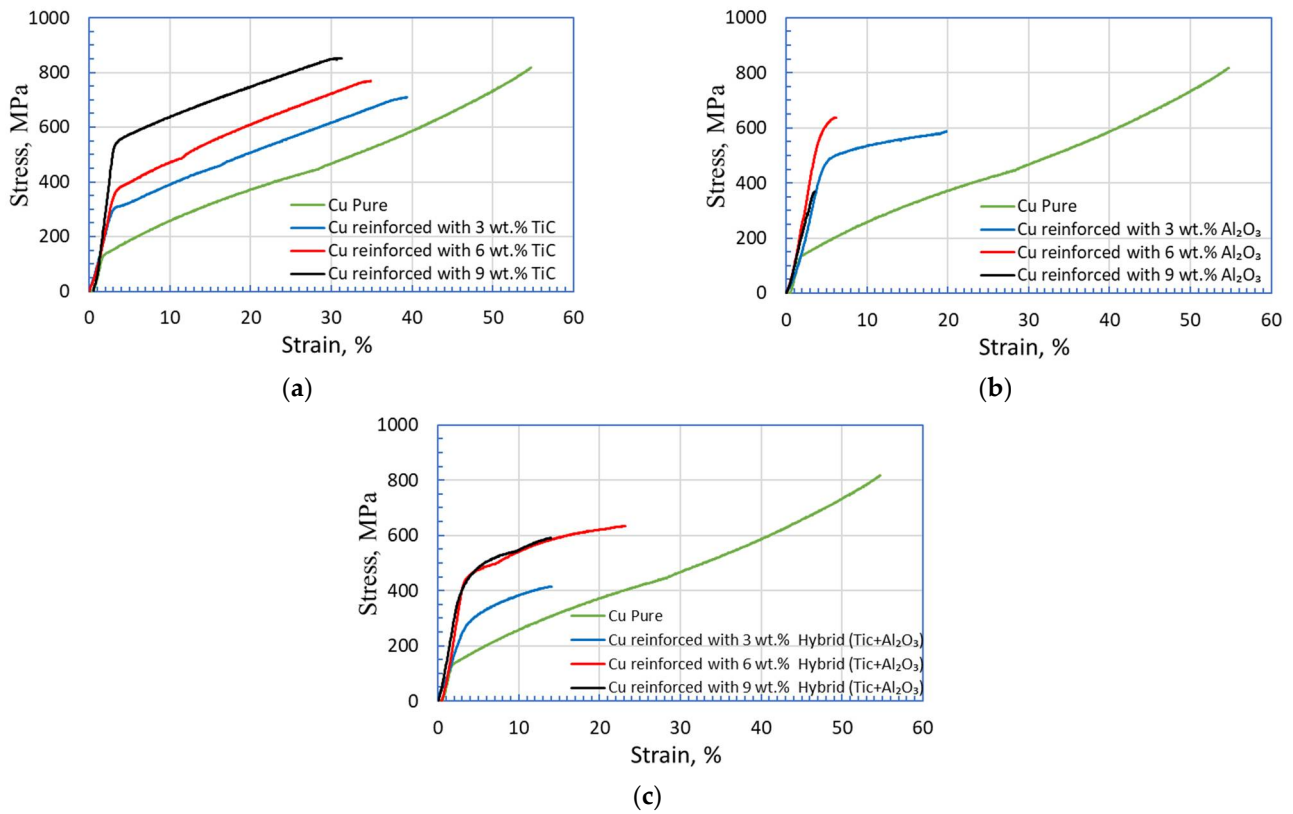


Figure 8. Compressive stress–strain curve for pure Cu and Cu-reinforced composites prepared by the spark plasma sintering route, (a) Cu/TiC composites, (b) Cu/Al₂O₃ composites, and (c) Cu/hybrid composite.

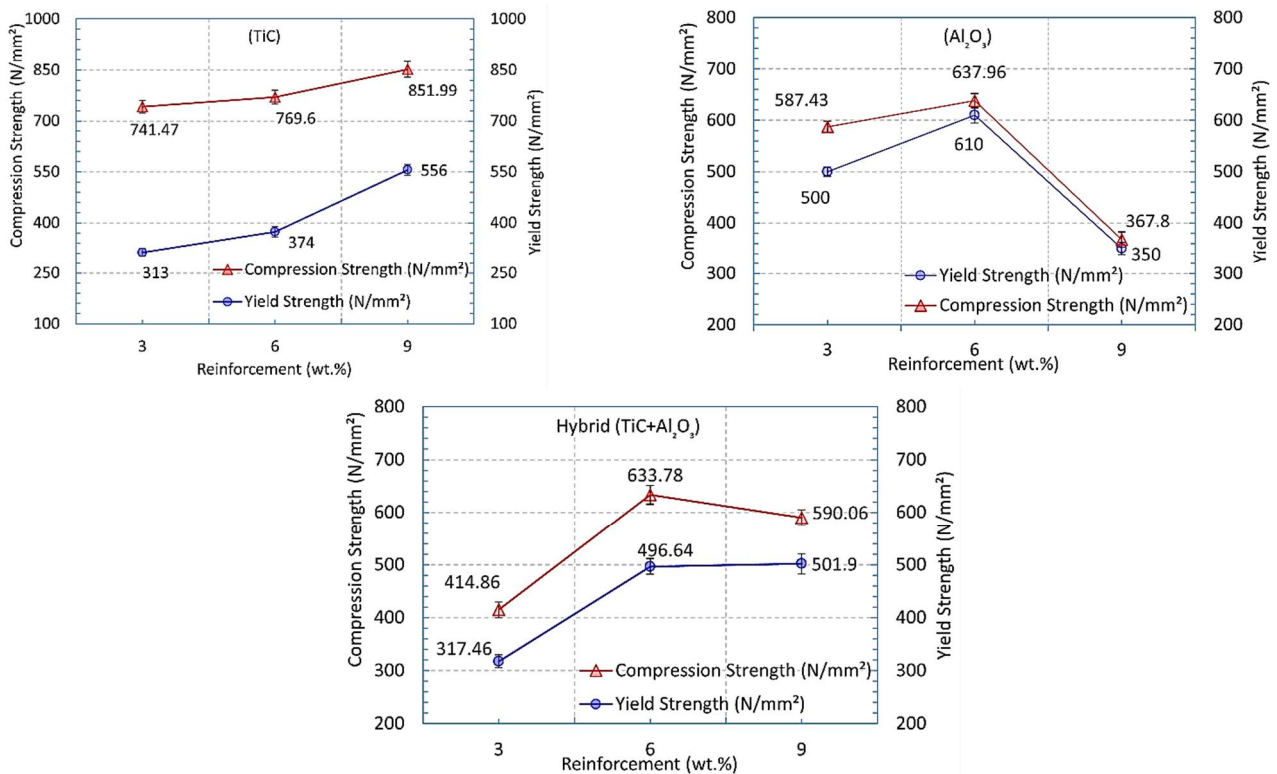


Figure 9. Effect of nanosized TiC and Al₂O₃ contents on the mechanical properties of the Cu-based composites prepared by spark plasma sintering.



Figure 10. Compressed test samples for pure Cu and Cu matrix nanocomposites.

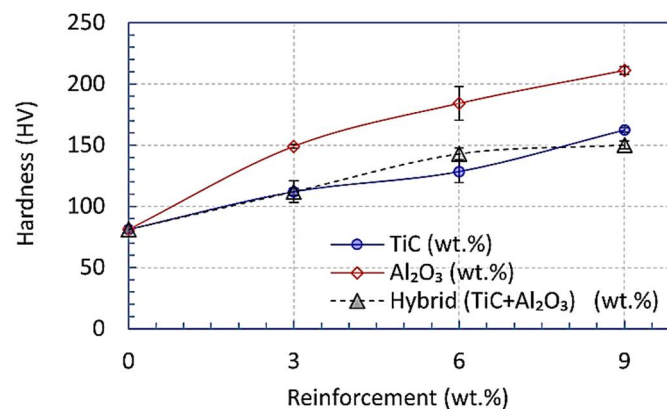


Figure 11. A diagram of the measured hardness for copper-based nanoceramics.

3.5. Strengthening Criteria

Increasing the strength of metallic materials is based on two competing factors. The first is work hardening, and the second is dynamic softening. Work hardening is caused by dislocations, multiplication, pileup, and tangle. Dynamic softening is caused by dislocations, rearrangement, and interactions. In the present work, the compression test and hardness measurement are carried out at room temperature, which is why the dynamic softening factor would not be probable, and the work hardening mechanism would affect the enhancement of strength and hardness. This is true for pure metal and alloys, unlike the composite materials where the contribution of ceramic additions to the matrix to enhance the properties should be considered.

Moreover, it is worth mentioning that some authors have considered the strengthening mechanisms in ceramic-reinforced composites [6,7,15,40,42–44]. The addition of TiC nanoparticles to the Cu matrix retained grain growth during sintering due to the peening effect of TiC for grain boundary movement and the strengthening effect of dispersed TiC in the Cu matrix grains where a mismatch of coefficient of thermal expansion is present [45] (see Figure 12). Furthermore, increasing the TiC fraction increased the strength and hardness of Cu-TiC composites in the present work. Another strengthening mechanism of TiC dispersion is the Orowan mechanism, especially at low fractions of TiC [6]. Compared to the other two cases, the composites with 3% and 6% Al₂O₃ gave the highest yield strength. This is a signal of increasing material strength with decreasing ductility. This may be attributed to the good adhesion between Cu matrix and TiC nanoparticles than between

Cu and Al_2O_3 [46]. An extreme drop in the Cu- Al_2O_3 composite strength is noticed at 9 wt.% of Al_2O_3 . This unexpected behavior may be attributed to the agglomeration of some alumina particles in the Cu matrix, increasing the chance for particle-to-particle contact (see Figure 13). A balanced behavior was observed with the hybrid ($\text{TiC}/\text{Al}_2\text{O}_3$) additions to the Cu matrix in which the combined effects of both ceramics are clear.

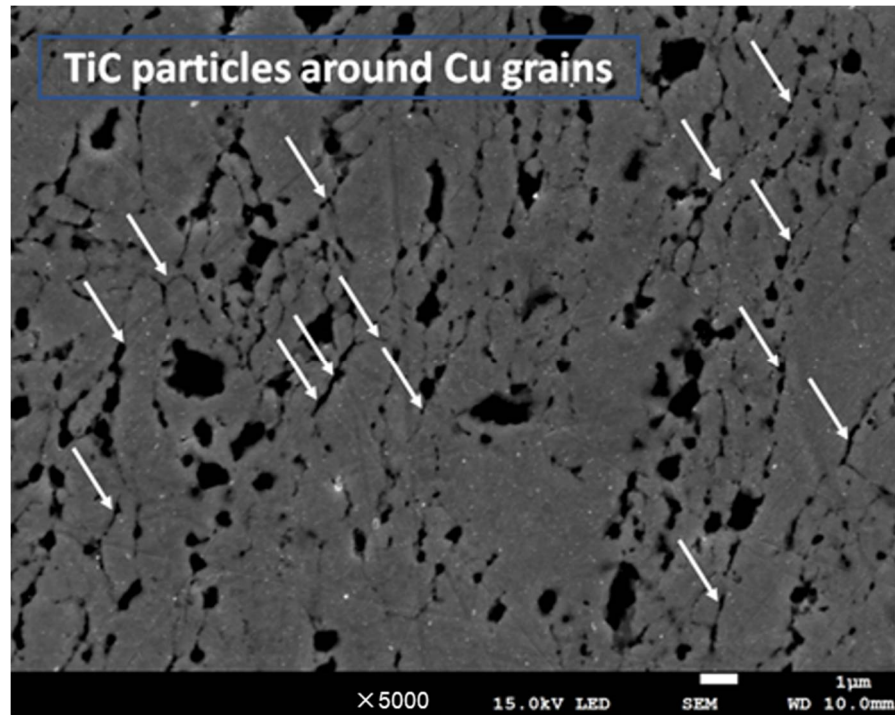


Figure 12. Spot white arrows indicate TiC around Cu grains.

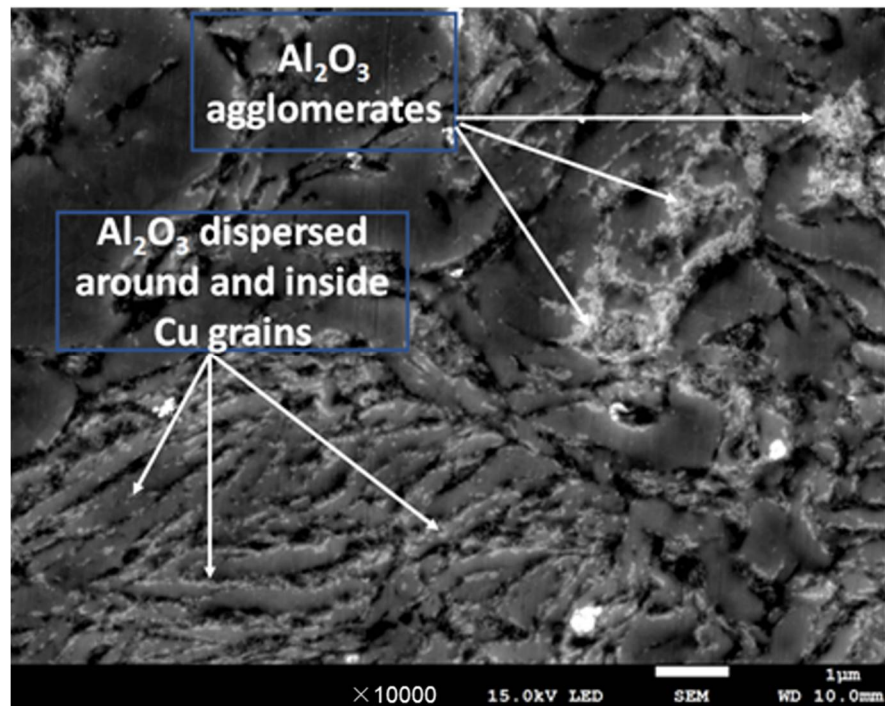


Figure 13. SEM showing alumina distribution behavior in the Cu matrix.

Reinforcing the Cu matrix, which is ductile in nature with two types of ceramic materials—ceramic carbide (TiC) and ceramic oxide (Al_2O_3)—helps to improve the mechanical properties of the Cu matrix. Both TiC and Al_2O_3 are at the nanoscale; therefore, by high ball milling, they filled the interstitial voids between Cu particles. As a consequence, the strengthening effect of both of them is distributed all over the Cu matrix. The hardness estimation test increased as the nano-ceramic hard particles were increased. This can also be explained by the resistance of the hard ceramic particles to the indenter from greater depth in the Cu-composite surface.

Consequently, the hardness is enhanced [46,47]. For the compression test, the presence of the nano-ceramic particles dispersed formally in the Cu matrix prevents the dislocation of the particles. In addition, as these hybrid reinforcements are at the nanoscale, they fill the voids; consequently, the strength of samples is increased [47–49].

Table 2 shows a comparison between the present study and previous work used to fabricate copper composites reinforced with alumina and titanium carbide nanoparticles. In this work, different concentrations of nano alumina and/or nano titanium carbide particles were used as a reinforcement material to the Cu matrix manufactured by the SPS technique. This work is compared with the same composites prepared by traditional sintering, vacuum sintering, hot pressing, and hot extrusion. The table shows that the composites produced by the SPS technique have the best mechanical properties compared with the other consolidation techniques.

Table 2. Comparing the present study with literature data of previous investigations.

Composite	Method	Density, (g/cm ³)	Ultimate Stress, (MPa)	Yield Stress, (MPa)	Elongation, (%)	Hardness, (HV)	Ref. No
Pure copper		97	N/A	127.15	1.69	81	
Cu-3 wt.% TiC	SPS at 950 °C	96	741.47	313	3.97	111.9	[Present study]
Cu-3 wt.% Al_2O_3		95	587.43	500	6.17	149	
Cu-1.5 wt.% TiC and 1.5 wt.% Al_2O_3		95	414.86	317.46	5.25	112	
Cu-5 wt.% TiC		Hot Press at 700 °C	93.3	N/A	N/A	N/A	
Cu-5 vol.%TiC	Hot extrusion	N/A	N/A	N/A	N/A	112	[51]
Cu-5 vol.% TiC	SPS	N/A	712	661	N/A	221	[14]
Cu-77 vol.% TiC	Sintering in Vacuum Furnace at 900 °C	93.4	N/A	N/A	N/A	544	[52]
Cu-5.3 vol.%TiC	SPS	N/A	602	572	N/A	194	[53]
Cu-3 wt.% Al_2O_3 with Coating Ag	Sintered at 950 °C	95.9	N/A	N/A	N/A	85	[7]
Cu-10 vol.% Al_2O_3	Sintered at 880 °C	83.49	N/A	N/A	N/A	71	[54]
Cu-3 vol.% Al_2O_3	Sintered at 850 °C	91.5	350	N/A	0.51	77	[55]
Cu-5 vol.% Al_2O_3	Sintered at 850 °C	88	550	N/A	0.46	100	
Cu-5 vol.% Al_2O_3	Sintering H2 at 850 °C		530	450	2.5	155	[56]
Cu-2.7 wt.% Al_2O_3	Sintered at 950 °C	92.53	460	350	N/A	54.83	[57]
Cu-5 vol.% Al_2O_3	Conventional Sintering N ₂	84.3	N/A	N/A	N/A	49	[58]
Cu-5 vol.% Al_2O_3	Conventional Sintering Ar	84.3	N/A	N/A	N/A	48	
Cu-5 vol.% Al_2O_3	Conventional Sintering H ₂	94.4	N/A	N/A	N/A	79	
Cu-5 vol.% Al_2O_3	SPS at 700 °C	92.2	N/A	N/A	N/A	125	
Cu-2.75 wt.% Al_2O_3	Pulsed Electric Current Sintered (PECS)	99.6	N/A	N/A	N/A	94.83	

4. Conclusions

Cu-(TiC and/or Al_2O_3) nanocomposites were synthesized successfully using mechanical milling followed by the spark plasma sintering (SPS) technique.

The density decreased with increasing percentages of the nano reinforcements (TiC and/or Al_2O_3). A maximum relative density of ~96% was achieved with the addition of 3 wt.% TiC to copper, whereas the minimum relative density (89%) was obtained by adding 9 wt.% Al_2O_3 to copper.

Agglomerated areas of Al₂O₃ nanoparticles around grain boundaries were observed, and increased with increasing Al₂O₃ fractions that, in turn, adversely affect the mechanical properties.

The compression strength of Cu/TiC increased with increasing the TiC fraction, and a maximum value of 851.99 N/mm² was obtained by Cu/9% TiC. A dramatic behavior was observed for Cu/Al₂O₃ composites that gave the minimum compressive strength of 367.8 N/mm² resulted at 9% Al₂O₃.

The maximum hardness of 211 HV was obtained by Cu/9% Al₂O₃, whereas two types of composites obtained the minimum hardness value of 112 HV: the Cu/3% TiC and Cu/3% hybrid.

Author Contributions: F.S.H.: investigation, writing—original draft and preparation; O.A.E.: Investigation, writing—original draft, review, and editing; A.R.S.E.: conceptualization and formal analysis; A.E.-N.: investigation and review; A.E.: methodology, review, and editing; A.K.E.: review and editing. All authors have read and agreed to the published version of the manuscript.

Funding: This research received no external funding.

Institutional Review Board Statement: Not applicable.

Informed Consent Statement: Not applicable.

Data Availability Statement: The data that support the findings of this study are included in the article. Any further requested information can be addressed to the corresponding author.

Acknowledgments: The authors acknowledge the kind support by Katsuyoshi Kondoh, Composite Materials Processing Lab., Osaka University, for providing the spark plasma sintering machine in his laboratory to carry out the consolidation of the composites and thank the researchers and technicians of the Central Metallurgical R & D Institute (CMRDI) in Cairo, Egypt for their collaboration.

Conflicts of Interest: The authors declare no potential conflict of interest concerning this article's research, authorship, and/or publication.

References

- Daghigh, R.; Oramipoor, H.; Shahidian, R. Improving the Performance and Economic Analysis of Photovoltaic Panel Using Copper Tubular-Rectangular Ducted Heat Exchanger. *Renew. Energy* **2020**, *156*, 1076–1088. [\[CrossRef\]](#)
- Abyzov, A.M.; Kidalov, S.V.; Shakhov, F.M. High Thermal Conductivity Composite of Diamond Particles with Tungsten Coating in a Copper Matrix for Heat Sink Application. *Appl. Therm. Eng.* **2012**, *48*, 72–80. [\[CrossRef\]](#)
- Xiao, Y.; Yao, P.; Zhou, H.; Zhang, Z.; Gong, T.; Zhao, L.; Deng, M. Investigation on Speed-Load Sensitivity to Tribological Properties of Copper Metal Matrix Composites for Braking Application. *Metals* **2020**, *10*, 889. [\[CrossRef\]](#)
- Cao, G.; Konishi, H.; Li, X. Mechanical Properties and Microstructure of Mg/SiC Nanocomposites Fabricated by Ultrasonic Cavitation Based Nanomanufacturing. *J. Manuf. Sci. Eng. Trans. ASME* **2008**, *130*, 0311051–0311056. [\[CrossRef\]](#)
- Kaftelen, H.; Ünlü, N.; Göller, G.; Lütfi Öveolu, M.; Henein, H. Comparative Processing-Structure-Property Studies of Al-Cu Matrix Composites Reinforced with TiC Particulates. *Compos. Part A Appl. Sci. Manuf.* **2011**, *42*, 812–824. [\[CrossRef\]](#)
- Morris, D.G. The Origins of Strengthening in Nanostructured Metals and Alloys. *Rev. Metal.* **2010**, *46*, 173–186. [\[CrossRef\]](#)
- Sadoun, A.M.; Mohammed, M.M.; Fathy, A.; El-Kady, O.A. Effect of Al₂O₃ Addition on Hardness and Wear Behavior of Cu-Al₂O₃ Electro-Less Coated Ag Nanocomposite. *J. Mater. Res. Technol.* **2020**, *9*, 5024–5033. [\[CrossRef\]](#)
- Zhang, Z.; Chen, D.L. Contribution of Orowan Strengthening Effect in Particulate-Reinforced Metal Matrix Nanocomposites. *Mater. Sci. Eng. A* **2008**, *483–484*, 148–152. [\[CrossRef\]](#)
- Chandrakanth, R.G.; Rajkumar, K.; Aravindan, S. Fabrication of Copper-TiC-Graphite Hybrid Metal Matrix Composites through Microwave Processing. *Int. J. Adv. Manuf. Technol.* **2010**, *48*, 645–653. [\[CrossRef\]](#)
- Fathy, A.; El-Kady, O. Thermal Expansion and Thermal Conductivity Characteristics of Cu-Al₂O₃ Nanocomposites. *Mater. Des.* **2013**, *46*, 355–359. [\[CrossRef\]](#)
- Elsayed, A.; Li, W.; El Kady, O.A.; Daoush, W.M.; Olevsky, E.A.; German, R.M. Experimental Investigations on the Synthesis of W-Cu Nanocomposite through Spark Plasma Sintering. *J. Alloys Compd.* **2015**, *639*, 373–380. [\[CrossRef\]](#)
- Shyu, R.F.; Ho, C.T. In Situ Reacted Titanium Carbide-Reinforced Aluminum Alloys Composite. *J. Mater. Process. Technol.* **2006**, *171*, 411–416. [\[CrossRef\]](#)
- Ni, J.; Li, J.; Luo, W.; Han, Q.; Yin, Y.; Jia, Z.; Huang, B.; Hu, C.; Xu, Z. Microstructure and Properties of In-Situ TiC Reinforced Copper Nanocomposites Fabricated via Long-Term Ball Milling and Hot Pressing. *J. Alloys Compd.* **2018**, *755*, 24–28. [\[CrossRef\]](#)
- Wang, F.; Li, Y.; Wang, X.; Koizumi, Y.; Kenta, Y.; Chiba, A. In-Situ Fabrication and Characterization of Ultrafine Structured Cu-TiC Composites with High Strength and High Conductivity by Mechanical Milling. *J. Alloys Compd.* **2016**, *657*, 122–132. [\[CrossRef\]](#)

15. Zhao, Q.; Gan, X.; Zhou, K. Enhanced Properties of Carbon Nanotube-Graphite Hybrid-Reinforced Cu Matrix Composites via Optimization of the Preparation Technology and Interface Structure. *Powder Technol.* **2019**, *355*, 408–416. [[CrossRef](#)]
16. Akbarpour, M.R.; Mousa Mirabad, H.; Khalili Azar, M.; Kakaei, K.; Kim, H.S. Synergistic Role of Carbon Nanotube and SiCn Reinforcements on Mechanical Properties and Corrosion Behavior of Cu-Based Nanocomposite Developed by Flake Powder Metallurgy and Spark Plasma Sintering Process. *Mater. Sci. Eng. A* **2020**, *786*, 139395. [[CrossRef](#)]
17. Akbarpour, M.R.; Alipour, S.; Farvizi, M.; Kim, H.S. Mechanical, Tribological and Electrical Properties of Cu-CNT Composites Fabricated by Flake Powder Metallurgy Method. *Arch. Civ. Mech. Eng.* **2019**, *19*, 694–706. [[CrossRef](#)]
18. Kumar, R.; Chaubey, A.K.; Bathula, S.; Jha, B.B.; Dhar, A. Synthesis and Characterization of Al₂O₃-TiC Nano-Composite by Spark Plasma Sintering. *Int. J. Refract. Met. Hard Mater.* **2016**, *54*, 304–308. [[CrossRef](#)]
19. Mohammadzadeh, A.; Akbarpour, M.R.; Heidarzadeh, A. Production of Nanostructured Copper Powder: Microstructural Assessments and Modeling. *Mater. Res. Express* **2018**, *5*, 065050. [[CrossRef](#)]
20. Akbarpour, M.R.; Alipour, S. Wear and Friction Properties of Spark Plasma Sintered SiC/Cu Nanocomposites. *Ceram. Int.* **2017**, *43*, 13364–13370. [[CrossRef](#)]
21. Hosseini, S.A.; Ranjbar, K.; Dehmolaei, R.; Amirani, A.R. Fabrication of Al5083 Surface Composites Reinforced by CNTs and Cerium Oxide Nano Particles via Friction Stir Processing. *J. Alloys Compd.* **2015**, *622*, 725–733. [[CrossRef](#)]
22. Fono-Tamo, R.S.; Tien-Chien, J.; Akinlabi, E.T.; Sanusi, K.O. Surface Characteristics of Stainless Steel Powder in Magnesium Substrate: A Friction Stir Processed Composite. In Proceedings of the IEEE 10th International Conference on Mechanical and Intelligent Manufacturing Technologies (ICMIMT 2019), Cape Town, South Africa, 15–17 February 2019; pp. 10–14. [[CrossRef](#)]
23. Mahmoud, E.R.I.; Ikeuchi, K.; Takahashi, M. Fabrication of SiC Particle Reinforced Composite on Aluminium Surface by Friction Stir Processing. *Sci. Technol. Weld. Join.* **2008**, *13*, 607–618. [[CrossRef](#)]
24. Tinubu, O.O.; Das, S.; Dutt, A.; Mogonye, J.E.; Ageh, V.; Xu, R.; Forsdike, J.; Mishra, R.S.; Scharf, T.W. Friction Stir Processing of A-286 Stainless Steel: Microstructural Evolution during Wear. *Wear* **2016**, *356–357*, 94–100. [[CrossRef](#)]
25. Escobar, J.D.; Velásquez, E.; Santos, T.F.A.; Ramirez, A.J.; López, D. Improvement of Cavitation Erosion Resistance of a Duplex Stainless Steel through Friction Stir Processing (FSP). *Wear* **2013**, *297*, 998–1005. [[CrossRef](#)]
26. Rathee, S.; Maheshwari, S.; Siddiquee, A.N.; Srivastava, M. Distribution of Reinforcement Particles in Surface Composite Fabrication via Friction Stir Processing: Suitable Strategy. *Mater. Manuf. Process.* **2018**, *33*, 262–269. [[CrossRef](#)]
27. Wen, H. *Processing, Microstructure, Mechanical Behavior and Deformation Mechanisms of Bulk Nanostructured Copper and Copper Alloys*; University of California: Davis, CA, USA, 2012.
28. Deng, H.; Yi, J.; Xia, C.; Yi, Y. Improving the Mechanical Properties of Carbon Nanotube-Reinforced Pure Copper Matrix Composites by Spark Plasma Sintering and Hot Rolling. *Mater. Lett.* **2018**, *210*, 177–181. [[CrossRef](#)]
29. Kim, K.T.; Cha, S.; Hong, S.H.; Hong, S.H. Microstructures and Tensile Behavior of Carbon Nanotube Reinforced Cu Matrix Nanocomposites. *Mater. Sci. Eng. A* **2006**, *430*, 27–33. [[CrossRef](#)]
30. Asgharzadeh, H.; Eslami, S. Effect of Reduced Graphene Oxide Nanoplatelets Content on the Mechanical and Electrical Properties of Copper Matrix Composite. *J. Alloys Compd.* **2019**, *806*, 553–565. [[CrossRef](#)]
31. Deng, H.; Yi, J.; Xia, C.; Yi, Y. Mechanical Properties and Microstructure Characterization of Well-Dispersed Carbon Nanotubes Reinforced Copper Matrix Composites. *J. Alloys Compd.* **2017**, *727*, 260–268. [[CrossRef](#)]
32. German, R.M. *Particulate Composites*; Springer International Publishing: Cham, Switzerland, 2016; ISBN 978-3-319-29915-0.
33. Nautiyal, H.; Srivastava, P.; Khatri, O.P.; Mohan, S.; Tyagi, R. Wear and Friction Behavior of Copper Based Nano Hybrid Composites Fabricated by Spark Plasma Sintering. *Mater. Res. Express* **2019**, *6*, 0850h2. [[CrossRef](#)]
34. Oanh, N.T.H.; Viet, N.H.; Kim, J.C.; Kim, J.S. Synthesis and Characterization of Cu-TiC Nanocomposites by Ball Milling and Spark Plasma Sintering. *Mater. Sci. Forum* **2014**, *804*, 173–176. [[CrossRef](#)]
35. Oanh, N.T.H.; Viet, N.H.; Kim, J.S.; Dudina, D.V. Structural Investigations of TiC-Cu Nanocomposites Prepared by Ball Milling and Spark Plasma Sintering. *Metals* **2017**, *7*, 123.
36. Fariás, I.; Olmos, L.; Jiménez, O.; Flores, M.; Braem, A.; Vleugels, J. Wear Modes in Open Porosity Titanium Matrix Composites with TiC Addition Processed by Spark Plasma Sintering. *Trans. Nonferrous Met. Soc. China* **2019**, *29*, 1653–1664. [[CrossRef](#)]
37. Abdel-Aziem, W.; Hamada, A.; Makino, T.; Hassan, M. Microstructural Evolution during Extrusion of Equal Channel Angular-Pressed AA1070 Alloy in Micro/Mesoscale. *Mater. Sci. Technol.* **2020**, *36*, 1169–1177. [[CrossRef](#)]
38. Zak, A.K.; Majid, W.A.; Abrishami, M.E.; Yousefi, R. X-Ray Analysis of ZnO Nanoparticles by Williamson-Hall and Size-Strain Plot Methods. *Solid State Sci.* **2011**, *13*, 251–256. [[CrossRef](#)]
39. Fathy, A.; Elkady, O.; Abu-Oqail, A. Production and Properties of Cu-ZrO₂ Nanocomposites. *J. Compos. Mater.* **2018**, *52*, 1519–1529. [[CrossRef](#)]
40. Sohag, M.A.Z.; Gupta, P.; Kondal, N.; Kumar, D.; Singh, N.; Jamwal, A. Effect of Ceramic Reinforcement on the Microstructural, Mechanical and Tribological Behavior of Al-Cu Alloy Metal Matrix Composite. *Mater. Today Proc.* **2020**, *21*, 1407–1411. [[CrossRef](#)]
41. Cavaliere, P. Spark Plasma Sintering of Materials: Advances in Processing and Applications. *Spark Plasma Sinter. Mater. Adv. Process. Appl.* **2019**, 1–781.
42. Pan, Y.; Xiao, S.Q.; Lu, X.; Zhou, C.; Li, Y.; Liu, Z.W.; Liu, B.W.; Xu, W.; Jia, C.C.; Qu, X.H. Fabrication, Mechanical Properties and Electrical Conductivity of Al₂O₃ Reinforced Cu/CNTs Composites. *J. Alloys Compd.* **2019**, *782*, 1015–1023. [[CrossRef](#)]
43. Tu, J.P.; Wang, N.Y.; Yang, Y.Z.; Qi, W.X.; Liu, F.; Zhang, X.B.; Lu, H.M.; Liu, M.S. Preparation and Properties of TiB₂ Nanoparticle Reinforced Copper Matrix Composites by in Situ Processing. *Mater. Lett.* **2002**, *52*, 448–452. [[CrossRef](#)]

44. Babapoor, A.; Asl, M.S.; Ahmadi, Z.; Namini, A.S. Effects of Spark Plasma Sintering Temperature on Densification, Hardness and Thermal Conductivity of Titanium Carbide. *Ceram. Int.* **2018**, *44*, 14541–14546. [[CrossRef](#)]
45. Yin, Z.; Huang, C.; Zou, B.; Liu, H.; Zhu, H.; Wang, J. Study of the Mechanical Properties, Strengthening and Toughening Mechanisms of Al₂O₃/TiC Micro-Nano-Composite Ceramic Tool Material. *Mater. Sci. Eng. A* **2013**, *577*, 9–15. [[CrossRef](#)]
46. Peng, T.; Yan, Q.; Zhang, X.; Zhuang, Y. Role of Titanium Carbide and Alumina on the Friction Increment for Cu-Based Metallic Brake Pads under Different Initial Braking Speeds. *Friction* **2021**, *9*, 1543–1557. [[CrossRef](#)]
47. Venkateswarlu, M.; Kumar, M.A.; Reddy, K.H.C. Thermal Behavior of Spark Plasma Sintered Ceramic Matrix-Based Nanocomposites. *J. Bio-Tribo-Corrosion* **2020**, *6*, 6013–6028. [[CrossRef](#)]
48. Wagih, A.; Abu-Oqail, A.; Fathy, A. Effect of GNPs Content on Thermal and Mechanical Properties of a Novel Hybrid Cu-Al₂O₃/GNPs Coated Ag Nanocomposite. *Ceram. Int.* **2019**, *45*, 1115–1124. [[CrossRef](#)]
49. Kumar, E.G.; Ahasan, M.; Venkatesh, K.; Sastry, K.S.B.S.V.S. Design, Fabrication of Powder Compaction Die and Sintered Behavior of Copper Matrix Hybrid Composite. *Int. Res. J. Eng. Technol.* **2018**, *5*, 876–882.
50. Akkaş, M.; Islak, S.; Özorak, C. Corrosion and Wear Properties of Cu-TiC Composites Produced by Hot Pressing Technique. *Celal Bayar Üniversitesi Fen Bilim. Derg.* **2018**, *14*, 465–469. [[CrossRef](#)]
51. Palma, R.H.; Sepúlveda, A.H.; Espinoza, R.A.; Montiglio, R.C. Performance of Cu-TiC Alloy Electrodes Developed by Reaction Milling for Electrical-Resistance Welding. *J. Mater. Process. Technol.* **2005**, *169*, 62–66. [[CrossRef](#)]
52. Akhtar, F.; Askari, S.J.; Shah, K.A.; Du, X.; Guo, S. Microstructure, Mechanical Properties, Electrical Conductivity and Wear Behavior of High Volume TiC Reinforced Cu-Matrix Composites. *Mater. Charact.* **2009**, *60*, 327–336. [[CrossRef](#)]
53. Wang, F.; Li, Y.; Yamanaka, K.; Wakon, K.; Harata, K.; Chiba, A. Influence of Two-Step Ball-Milling Condition on Electrical and Mechanical Properties of TiC-Dispersion-Strengthened Cu Alloys. *Mater. Des.* **2014**, *64*, 441–449. [[CrossRef](#)]
54. Öksüz, K.E.; Şahin, Y. Microstructure and Hardness Characteristics of Al₂O₃-B₄C Particle-Reinforced Cu Matrix Composites. *Acta Phys. Pol. A* **2016**, *129*, 650–652. [[CrossRef](#)]
55. Panda, S.; Dash, K.; Ray, B.C. Processing and Properties of Cu Based Micro- and Nano-Composites. *Bull. Mater. Sci.* **2014**, *37*, 227–238. [[CrossRef](#)]
56. Orolínová, M.; Ďurišin, J.; Ďurišinová, K.; Danková, Z.; Ďurišin, M. Effect of Microstructure on Properties of Cu-Al₂O₃ Nanocomposite. *Chem. Mater. Eng.* **2013**, *1*, 60–67. [[CrossRef](#)]
57. Fathy, A.; Shehata, F.; Abdelhameed, M.; Elmahdy, M. Compressive and Wear Resistance of Nanometric Alumina Reinforced Copper Matrix Composites. *Mater. Des.* **2012**, *36*, 100–107. [[CrossRef](#)]
58. Dash, K.; Ray, B.C.; Chaira, D. Synthesis and Characterization of Copper-Alumina Metal Matrix Composite by Conventional and Spark Plasma Sintering. *J. Alloys Compd.* **2012**, *516*, 78–84. [[CrossRef](#)]
59. Ritasalo, R.; Liu, X.W.; Söderberg, O.; Keski-Honkola, A.; Pitkänen, V.; Hannula, S.P. The Microstructural Effects on the Mechanical and Thermal Properties of Pulsed Electric Current Sintered Cu-Al₂O₃ Composites. *Procedia Eng.* **2011**, *10*, 124–129. [[CrossRef](#)]